catalysts

MDPI

Article

Exploring the Effect of the Solvothermal Time on the Structural Properties and Catalytic Activity of Cu-ZnO-ZrO_2 Catalysts Synthesized by the Solvothermal Method for CO_2 Hydrogenation to Methanol

Jian Han, Yannan Liang, Jun Yu, Guisheng Wu and Dongsen Mao *

School of Chemical and Environmental Engineering, Shanghai Institute of Technology, Shanghai 201418, China
* Correspondence: dsmao@sit.edu.cn; Tel./Fax: +86-21-6087-7231

Abstract: A series of Cu-ZnO-ZrO_2 (CCZ) catalysts were prepared by the solvothermal method with different solvothermal times (1 h, 3 h, 6 h, and 12 h). The physicochemical properties of these catalysts and the catalytic performance for CO_2 hydrogenation to methanol were studied. The highest methanol yield was achieved when the solvothermal time was 6 h (CCZ-6). Furthermore, we found that the copper surface area (S_{Cu}) increases and then decreases with an increase in the solvothermal time and that there is a strong correlation between the methanol yield and the S_{Cu}. This research highlights the crucial influence of the solvothermal time on the structure and catalytic behavior of Cu-ZnO-ZrO_2 catalysts, providing a valuable reference for the development of efficient catalysts.

Keywords: Cu-ZnO-ZrO_2; solvothermal times; copper surface area; methanol yield; CO_2 hydrogenation

Citation: Han, J.; Liang, Y.; Yu, J.; Wu, G.; Mao, D. Exploring the Effect of the Solvothermal Time on the Structural Properties and Catalytic Activity of Cu-ZnO-ZrO_2 Catalysts Synthesized by the Solvothermal Method for CO_2 Hydrogenation to Methanol. *Catalysts* **2024**, *14*, 390. https://doi.org/10.3390/catal14060390

Academic Editor: Jacek Grams

Received: 27 May 2024
Revised: 12 June 2024
Accepted: 15 June 2024
Published: 18 June 2024

1. Introduction

With the continuous growth of global energy demand and the increasing severity of environmental problems, the exploration of renewable energy sources and the reduction of greenhouse gas emissions have become important issues that need to be urgently addressed [1]. Among the greenhouse gases, the conversion and utilization of carbon dioxide (CO_2) has received much attention [2,3]. Methanol (CH_3OH) has gradually gained recognition as a clean and renewable fuel source by global industry due to its widespread availability, significant economic volume, and sustainable development of the whole industrial chain [4,5]. Therefore, among the many ways to convert CO_2, the conversion of CO_2 to methanol by the hydrogenation reaction is a prospective solution [6–8].

Copper-based catalysts have become a popular research topic due to their low cost and high catalytic activity for the CO_2 hydrogenation to methanol reaction [9,10]. Among them, Cu-ZnO-ZrO_2 ternary catalysts have attracted much attention due to their exceptional catalytic performance [11–13]. Witoon et al. [13] claimed that the doping of graphene oxide significantly improved the catalytic performance of CuO-ZnO-ZrO_2 catalysts. Chang et al. [14] demonstrated that the ZnO/ZrO_2 composition in Cu/ZnO/ZrO_2 catalyst impacted CuZn alloy formation and surface basic sites, and the suitable ZnO/ZrO_2 composition significantly enhanced the catalytic activity and the methanol yield produced by CO_2 hydrogenation.

It has been shown that the preparation methods and conditions of catalysts have a significant effect on their structures and properties [15]. As we all know, the most commonly used method for the preparation of methanol synthesis catalysts is co-precipitation. The co-precipitation method involves the simultaneous precipitation of multiple components from a solution, leading to well-mixed and homogeneously distributed precursors [7,11]. However, the co-precipitation process is very sensitive to the conditions of the pH, temperature, and stirring speed of the solution, and a little carelessness may lead to the non-uniform

particle size distribution of the precipitates, which may in turn affect the performance of the catalyst. The solvothermal method, as an alternative effective synthesis method, can prepare nanomaterials with high dispersibility and excellent catalytic properties under relatively mild conditions [16,17]. Specifically, the time of the solvothermal treatment, as a key parameter in the solvothermal method, plays a crucial role in regulating the physicochemical properties of the catalyst [18,19]. A previous study [16] has shown that the solvothermal temperature has a significant effect on the structure of Cu-ZnO-ZrO_2 catalysts, and CCZ-180 with a solvothermal temperature of 180 °C had the best catalytic activity. However, the effect of the solvothermal time on the catalyst performance is equally important and needs to be further studied.

In this paper, a series of Cu-ZnO-ZrO_2 catalysts were prepared by the solvothermal method under different solvothermal times (1 h, 3 h, 6 h, and 12 h). The catalysts were analyzed via characterizations such as XRD, SEM, EDX mapping, N_2 adsorption–desorption, N_2O chemisorption, XPS, H_2-TPR, and CO_2/H_2-TPD. Furthermore, the relationships between the catalytic performance and the physicochemical properties were studied in detail.

2. Results and Discussion

2.1. Characterization

2.1.1. XRD

Figure 1 shows the XRD patterns of the calcined and reduced Cu-ZnO-ZrO_2 catalysts. From Figure 1a, the diffraction peaks at 2θ of 35.5°, 38.7°, 48.8°, 61.6°, 66.3°, 68.1°, and 75.0°, respectively, can be attributed to the presence of the CuO phase (PDF #48-1548), whereas the diffraction peaks appearing at 2θ = 30.3° correspond to tetragonal ZrO_2 (t-ZrO_2) (PDF #050-1089). No diffraction peak of ZnO was found in any of the four catalysts, indicating that ZnO was highly dispersed or existed in an amorphous state in all four catalysts [20,21].

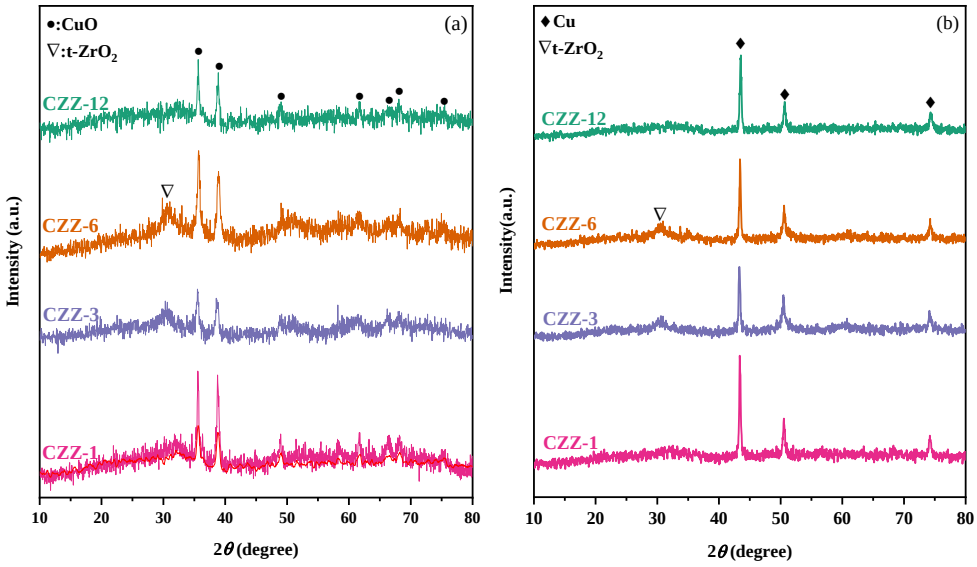

Figure 1. XRD patterns of the different Cu-ZnO-ZrO_2 catalysts: (**a**) calcined, and (**b**) reduced.

As shown in Figure 1b, after reduction at 300 °C, several peaks were observed at 2θ of 43.3°, 50.4°, and 74.1°, representing the crystalline surfaces of Cu(111), Cu(200), and Cu(220), respectively [22]. However, no peaks of CuO were found, suggesting that the CuO in these samples had been reduced [23]. The sizes of the metallic Cu and CuO crystals were determined by Scherer's formula and the results are summarized in Table 1. It can be observed that the sizes of both CuO and metallic Cu first decrease and then increase with the extension of the solvothermal time. Especially, CZZ-6 exhibited the smallest size of copper species, which improved the dispersion and increased the surface area, as evidenced by the maximum S_{BET} and S_{Cu} of CZZ-6. On the other hand, the sizes of metallic Cu are

noticeably larger than those of CuO for the same catalysts, and the most plausible reason for this phenomenon is that the reduction of CuO to metallic Cu with H_2 is an exothermic process ($CuO + H_2 \rightarrow Cu + H_2O$, $\Delta H = -129.2$ kJ/mol), and the heat released makes the metallic Cu particles aggregate and become larger. This phenomenon has also been reported in previous studies [17,24].

Table 1. Physicochemical properties of different Cu-ZnO-ZrO_2 catalysts.

Catalyst	S_{BET} (m^2/g)	Pore Volume (cm^3/g)	Pore Diameter (nm)	d_{CuO} [1] (nm)	d_{Cu} [1] (nm)	S_{Cu} [2] (m^2/g)
CZZ-1	20.7	0.055	10.6	26.8	30.2	4.6
CZZ-3	32.7	0.069	8.1	22.2	27.2	12.0
CZZ-6	40.5	0.087	8.6	19.1	25.7	15.7
CZZ-12	16.4	0.054	13.3	27.7	29.1	4.5

[1] Determined by XRD. [2] Determined by the N_2O chemisorption method.

2.1.2. SEM and EDX Mapping

Figure 2 shows SEM images of the representative CZZ-6 sample. It can be seen that CZZ-6 is a built-up structure consisting of many particles that form a loose microstructure. An EDX mapping analysis was performed to investigate the distribution of the elements. It was confirmed that all the Cu, Zn, and Zr atoms in CCZ-6 are well-dispersed on the catalyst surface.

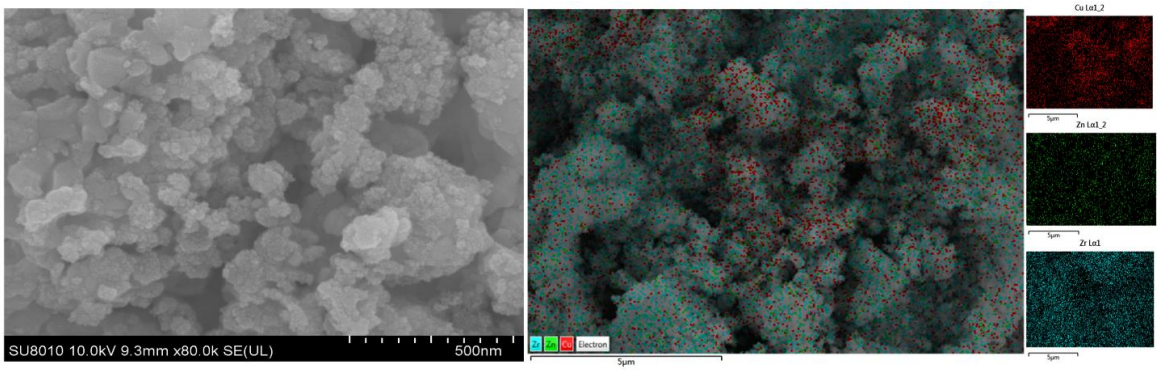

Figure 2. SEM and EDX mapping images of CCZ-6.

2.1.3. N_2 Adsorption–Desorption

The N_2 adsorption–desorption isotherms and pore size distribution curves for the different catalysts are shown in Figure 3. Clearly, all the samples showed type IV isotherms with H3-type hysteresis loops (Figure 3a), indicating that all the catalysts were mesoporous materials [25,26]. Furthermore, the hysteresis return line of CZZ-6 was larger than that of the other catalysts, indicating that it had the largest mesopore volume. As can be seen in Figure 3b, all four samples exhibited wide pore distributions, except for the concentration of pores at 1.9 nm, where the pore sizes gradually increased in the order of CZZ-3 < CZZ-6 < CZZ-1 < CZZ-12. These results indicate that the CZZ-3 catalyst had the narrowest pore distribution among the four catalysts.

The effects of the solvothermal time on the pore structure and specific surface area (S_{BET}) of the Cu-ZnO-ZrO_2 catalysts are listed in Table 1. As the solvothermal time increases, the S_{BET} and pore volume of the catalyst initially increase and then decrease. This result is consistent with the order of CuO particle size measured by XRD (Table 1). The CZZ-6 catalyst, with a solvothermal time of 6 h, possesses the largest S_{BET} and pore volume. A larger pore volume and S_{BET} could enhance the adsorption and desorption of the reaction gases, thereby improving the catalytic performance [27].

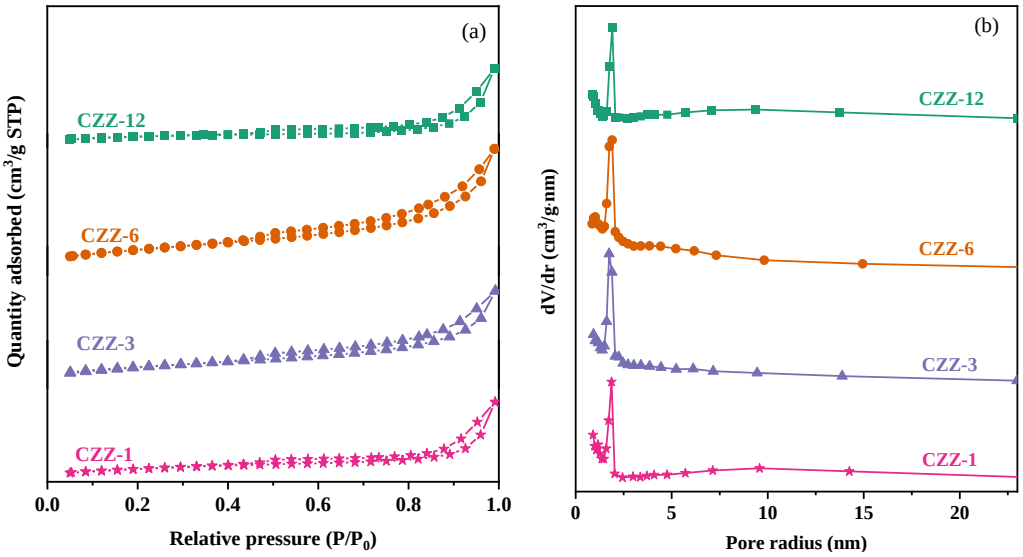

Figure 3. N_2 adsorption–desorption isotherms (**a**) and the corresponding pore size distribution curves (**b**) of the different Cu-ZnO-ZrO_2 catalysts.

2.1.4. S_{Cu}

The S_{Cu} of Cu-based catalysts has an important effect on the catalytic performance [12,27,28], so the N_2O chemisorption method was employed to determine the S_{Cu} of the different Cu-ZnO-ZrO_2 catalysts. As shown in Table 1, with the extension of the solvothermal time, the S_{Cu} first increases and then decreases. This trend is consistent with the change in the S_{BET} of the catalyst, with both reaching their maximum values in the CZZ-6 catalyst prepared with a solvothermal time of 6 h. The subsequent activity test results (Section 2.2) revealed that the larger the S_{Cu}, the better the catalytic activity that could be achieved. Especially, the CZZ-6 had the largest S_{Cu}, implying more highly dispersed copper particles [27,29], which was confirmed by its smallest copper particle size (d_{Cu}) in Table 1.

2.1.5. XPS

Figure 4 presents the XPS spectra of the copper species after calcination and in situ reduction. As depicted in Figure 4a, the peaks of the copper species appeared around 933 eV and 953 eV, with broad vibrational peaks appearing within 940–945 eV, indicating the presence of copper species in the form of Cu^{2+} [30]. Following in situ reduction at 300 °C (Figure 4b), the vibrational peaks disappeared and the signal peak of the copper species became narrower and shifted to lower binding energies at around 932 eV, suggesting the reduction of Cu^{2+} to Cu^0 and/or Cu^+ [31].

The Cu LMM XAES spectra of the Cu species were used to further distinguish between Cu^0 and Cu^+. From Figure 5, it can be observed that the CZZ-1 and CZZ-12 catalysts exhibited two overlapping peaks, indicating the coexistence of Cu^+ and Cu^0 species on the catalyst surface [32]. In contrast, only Cu^0 species were observed at the binding energy of 919.0 eV for CZZ-3 and CZZ-6. On the other hand, the characteristic peaks of Cu^+ were not observed in CZZ-1 and CZZ-12 according to the XRD analysis (Figure 1), possibly due to the amorphous nature of Cu_2O or its high dispersion.

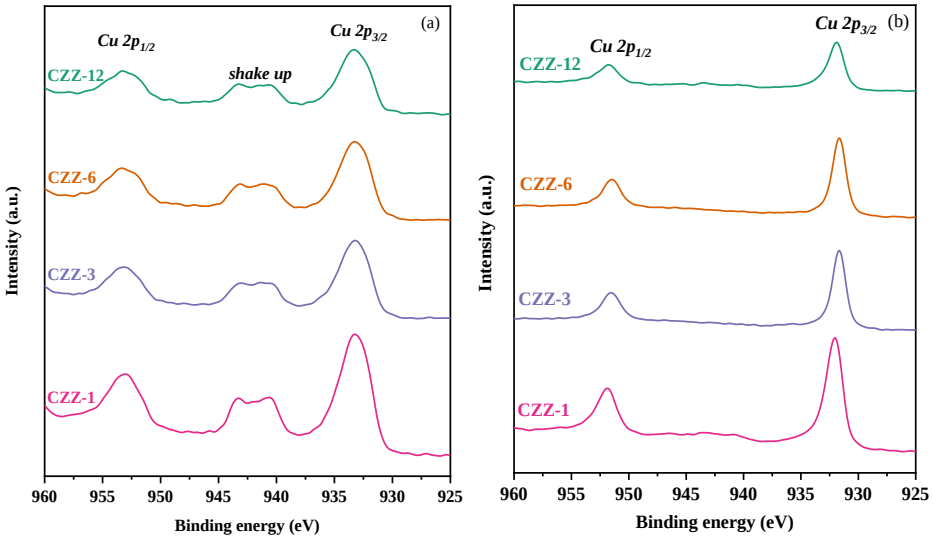

Figure 4. Cu 2p XPS spectra of the (**a**) calcined and (**b**) in situ reduced catalysts.

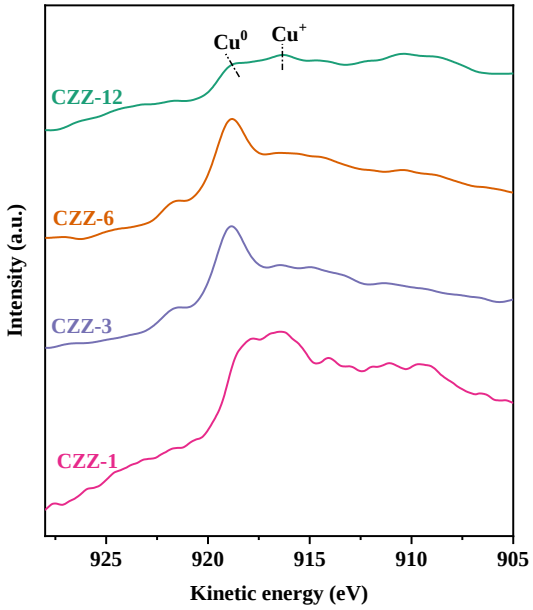

Figure 5. Cu LM2 XAES spectra of the in situ reduced catalysts.

Figure 6 shows the O 1s XPS spectra of the Cu-ZnO-ZrO_2 catalysts after in situ reduction. Three peaks were present on the spectra of all the catalysts: the α peak at 529 eV represented the lattice oxygen of the metal oxides, the β peak was the chemisorbed oxygen species, and the γ peak was the hydroxyl-like species [33]. Among them, the β and γ peaks were considered to be active sites and played an important role in CO_2 hydrogenation to methanol [34,35]. From Table S1, the largest $A_\beta + A_\gamma$ value was found in CZZ-6, which provided the foundation for the high activity.

The binding energy values and surface contents of the catalyst surfaces before and after in situ reduction are illustrated in Table S2. From Table S2, it can be seen that the binding energy values of Zn $2p_{3/2}$ were in the range of 1021.3–1021.5 eV, and those of Zr $3d_{5/2}$ were in the range of 181.7–181.9 eV, and there was no significant change in the binding energy values of Zn $2p_{3/2}$ and Zr $3d_{5/2}$ before and after in situ reduction, which indicated that Zn and Zr existed in the catalyst in the form of oxides and would not be reduced at 300 °C under a hydrogen atmosphere. Moreover, with the extension of the solvothermal time, the copper content on the catalyst surface followed the order: CZZ-1 > CZZ-3 > CZZ-6 > CZZ-12, while

the S_{Cu} order was: CZZ-12 < CZZ-1 < CZZ-3 < CZZ-6. Generally, the larger the copper content on the catalyst surface, the smaller the S_{Cu}. Clearly, in our study, there was no direct correlation between the copper content on the catalyst surface and the S_{Cu}. This discrepancy may be due to the aggregation of copper particles on the surface of the CZZ-12 with a prolonged solvothermal time, resulting in the smallest S_{Cu}.

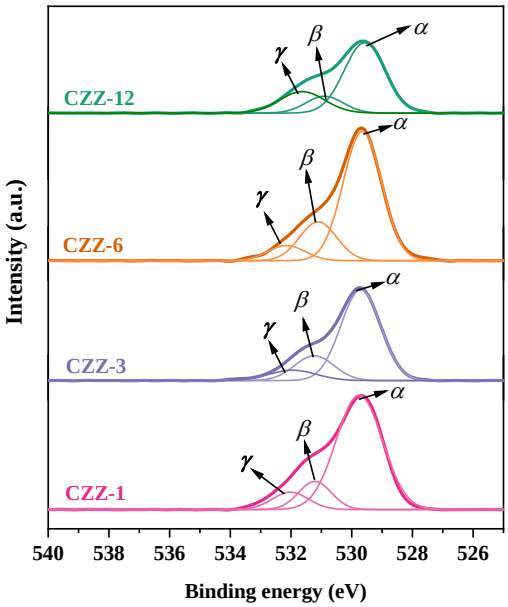

Figure 6. O 1s spectra of the in situ reduced catalysts.

2.1.6. H_2-TPR

The reduction properties of the Cu-ZnO-ZrO_2 catalysts were studied by H_2-TPR. As shown in Figure 7, all the catalysts showed a broad reduction peak between 150 and 300 °C. As mentioned earlier, ZnO and ZrO_2 were not reduced at 300 °C, and therefore, the peak was attributed to the reduction of the CuO_x species [7].

The small shoulder peak (α peak) on the low-temperature side can be clearly observed in the CZZ-1, and this result indicated that there were two different sizes of CuO particles in the CZZ-1. Unlike CZZ-1, the reduction peaks of the CZZ-3, CZZ-6, and CZZ-12 catalysts were relatively symmetrical, indicating that the CuO crystal sizes on these three catalysts were more uniform than those on CZZ-1. Furthermore, CZZ-6 was observed to have the lowest reduction temperature (202 °C) for CuO_x species. Low-temperature reduction usually indicates strong interactions between the metal and the oxide in the catalyst, which can enhance the dispersion of the metal species and make the reduction process easier to carry out [36–38]. Table 2 displays the quantitative data of the hydrogen consumption of the CuO-ZnO-ZrO_2 catalysts. It is observed that CZZ-1 and CZZ-3 have similar H_2 consumption, while CZZ-6 and CZZ-12 have more H_2 consumption, which suggests the presence of more reducible CuO_x species in CZZ-6 and CZZ-12. Furthermore, the H_2 consumption of all the catalysts was lower than the theoretical value required for the complete reduction of copper oxide to the metal Cu (the degree of the reduction was less than 1), further confirming that ZnO and ZrO_2 were not reduced. It has been well-documented that Cu-based catalysts with high activity for CO_2 hydrogenation to methanol have high reducibility [39,40]. CZZ-6 was expected to exhibit the highest activity due to its optimal reducibility among the four catalysts, as confirmed by the results of the activity tests (Section 2.2).

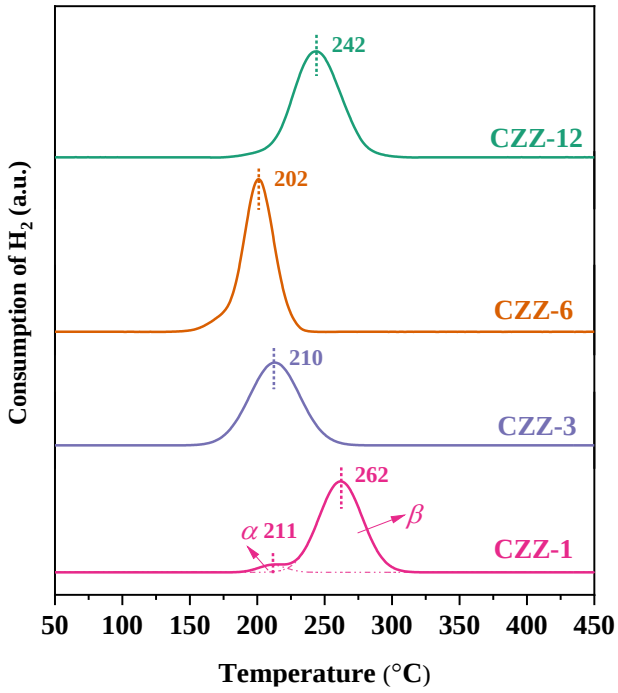

Figure 7. H_2-TPR patterns of the various catalysts.

Table 2. The temperature and H_2 consumption in the H_2-TPR patterns of the various catalysts.

Catalyst	Temperature of Peaks (°C)		H_2 Consumption of Peaks (μmol/g)			Degree of Reduction [1]
	T_α	T_β	α	β	Total	
CZZ-1	211	262	138	2676	2814	0.81
CZZ-3	210	-	2802	-	2802	0.80
CZZ-6	201	-	3306	-	3306	0.94
CZZ-12	242	-	3378	-	3378	0.96

[1] Determined by the ratio of the actual H_2 consumption of the catalysts to the theoretical H_2 consumption.

2.1.7. CO_2-TPD

The adsorption capacity of the catalysts for CO_2 was determined through CO_2-TPD. Figure 8 illustrates the CO_2-TPD profiles of the pre-reduced Cu-ZnO-ZrO_2 catalysts. It is observed that all the catalysts exhibited three CO_2 desorption peaks, which were deconvolved Gaussian peaks designated as α, β, and γ peaks, respectively. The low-temperature α peak corresponds to the desorption of CO_2 from weak basic sites associated with hydroxyl functional groups. The β peak represents the desorption of CO_2 from medium basic sites formed by the combination of metal and oxygen. The γ peak corresponds to the desorption of CO_2 from strong basic sites associated with low-coordination oxygen anions [16]. The CO_2 desorption data for different Cu-ZnO-ZrO_2 catalysts are presented in Table 3. It can be observed that the CZZ-3 and CZZ-6 catalysts exhibit larger CO_2 desorption ($A_\alpha + A_\beta + A_\gamma$ values), but the strength of the basic sites of the CZZ-6 is relatively weak compared to CZZ-3. The total desorption of CO_2 is crucial for the production of methanol by CO_2 hydrogenation [25], which will be discussed in Section 2.3.

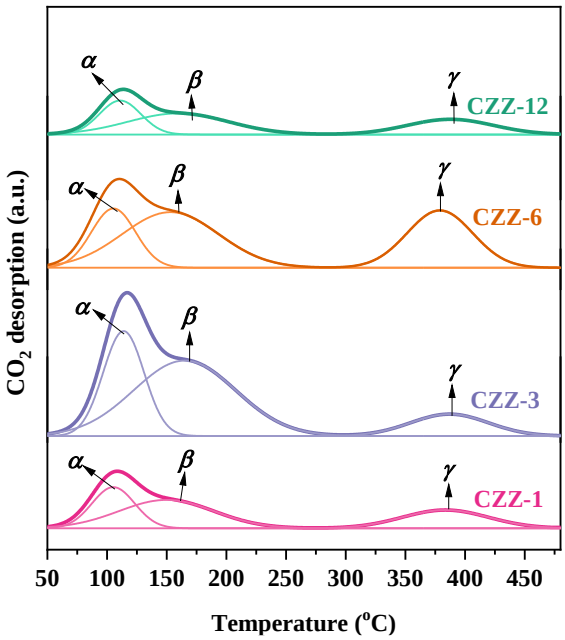

Figure 8. CO_2-TPD profiles of the pre-reduced catalysts.

Table 3. The data of the CO_2-TPD profiles of the different Cu-ZnO-ZrO_2 catalysts.

Catalyst	α Peak		β Peak		γ Peak		$(A_\alpha + A_\beta + A_\gamma)$/(a.u.)
	T_α/(°C)	A_α/(a.u.)	T_β/(°C)	A_β/(a.u.)	T_γ/(°C)	A_γ/(a.u.)	
CZZ-1	105	47	150	72	387	42	161
CZZ-3	114	116	165	207	389	46	369
CZZ-6	105	70	151	144	380	101	315
CZZ-12	111	46	160	68	390	42	156

2.1.8. H_2-TPD

Figure 9 displays the H_2-TPD profiles of the pre-reduced Cu-ZnO-ZrO_2 catalysts. The desorption peaks on the catalysts represent the H species adsorbed on the surface of the active component Cu [15,27]. It is generally observed that the low-temperature α peak represents the desorption of undissociated molecular hydrogen (H_2) weakly adsorbed on the catalyst surface, while the high-temperature β peak represents the desorption of dissociated atomic hydrogen (H) [41]. The quantitative data for the temperature and peak area of the H_2 desorption peaks are listed in Table 4. Clearly, the temperatures of the α and β desorption peaks show irregular changes with the prolongation of the solvothermal time. However, the lowest desorption peak temperature of CZZ-6 indicates the weakest adsorption strength of H_2. On the other hand, with the extension of the solvothermal time, the peak areas of the α and β peaks first increased and then decreased, with the largest peak area observed at 6 h of solvothermal time. The maximum peak area of CZZ-6 indicates its highest H_2 adsorption capacity.

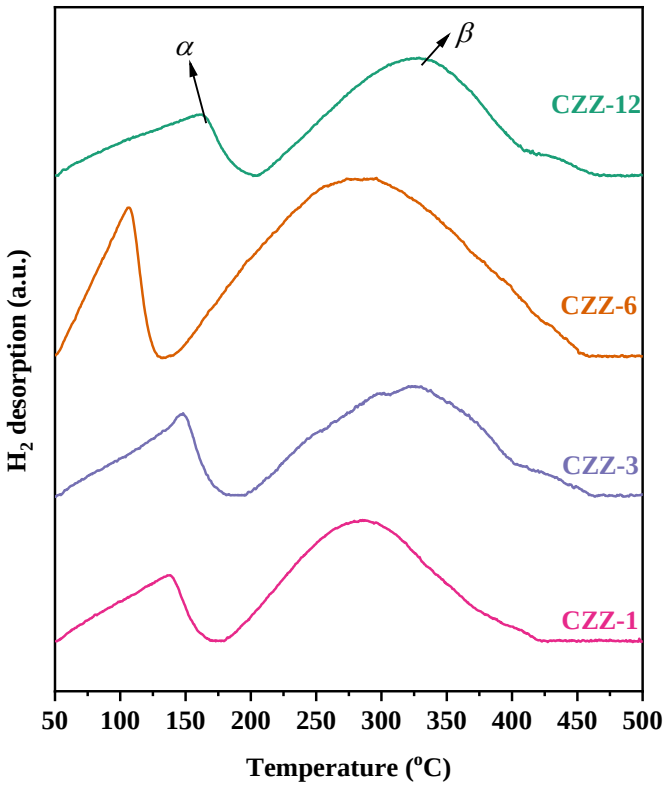

Figure 9. H_2-TPD profiles of the pre-reduced catalysts.

Table 4. The data of the H_2-TPD profiles of the different Cu-ZnO-ZrO_2 catalysts.

Catalyst	α Peak		β Peak		$A_\alpha + A_\beta$/(a.u.)
	T_α/(°C)	A_α/(a.u.)	T_β/(°C)	A_β/(a.u.)	
CZZ-1	137	20	285	80	100
CZZ-3	148	25	324	81	106
CZZ-6	106	30	282	172	202
CZZ-12	161	25	327	82	107

2.2. Catalytic Activity

Figure 10 presents the activity evaluation results of the Cu-ZnO-ZrO_2 catalysts prepared with different solvothermal times in the CO_2 hydrogenation to methanol. Under the current reaction conditions, CO and methanol were detected as carbon-containing reaction products. However, with the extension of the solvothermal time, the CO_2 conversion and methanol yield first increased and then decreased. CZZ-1 and CZZ-12 had low CO_2 conversion despite the high methanol selectivity, resulting in low methanol yields. The CO_2 conversion of CZZ-6 was 15.6%, with methanol selectivity of 46.1%, and the methanol yield reached a maximum of 7.2%. This indicates that the catalyst prepared with 6 h of solvothermal time is most suitable for methanol production.

To provide a comprehensive context for our catalytic activity results, we compared our findings with similar Cu-Zn-Zr catalysts reported in the literature for CO_2 hydrogenation to methanol. The comparison is summarized in Table S3 in the Supplementary Materials. It is well known that the performance of Cu-Zn-Zr catalysts for CO_2 hydrogenation heavily depends on factors such as the composition, pressure, temperature, H_2/CO_2 ratio, and feed gas space velocity [27,31]. Nevertheless, under similar reaction conditions, our CCZ-6 catalyst demonstrated comparable or even superior methanol yields. Our study indicates that optimizing the reaction time during solvothermal synthesis can effectively enhance the catalytic performance for CO_2 hydrogenation to methanol.

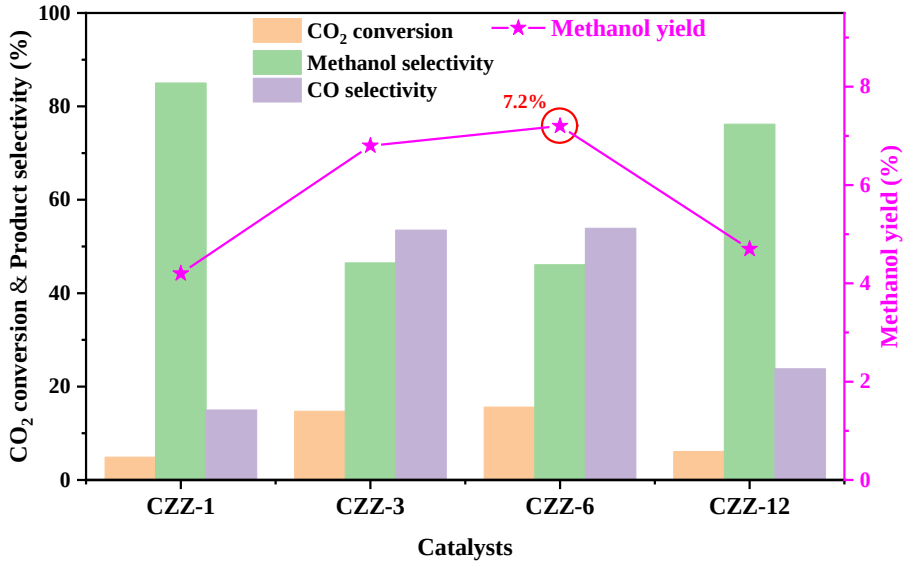

Figure 10. Catalytic performance of the different Cu-ZnO-ZrO_2 catalysts. Reaction conditions: P = 3.0 MPa, H_2:CO_2 = 3 (*v*/*v*), T = 240 °C, GHSV = 2400 mL/(g_{cat}·h).

2.3. Structure–Activity Relationship Analysis

As mentioned in relation to CO_2-TPD, the amount of CO_2 adsorbed by the different catalysts was observed to be clearly different. The adsorption of CO_2 is a pre-condition for conducting CO_2 hydrogenation [25,27]. The total CO_2 adsorption is an important index in the evaluation of high-performance catalysts. Therefore, the effect of the total amount of desorbed CO_2 on the methanol yield was investigated (Figure 11a). However, the relationship was not completely linear (R^2 = 0.79), which indicated that the amount of CO_2 absorbed was not directly responsible for the methanol yield.

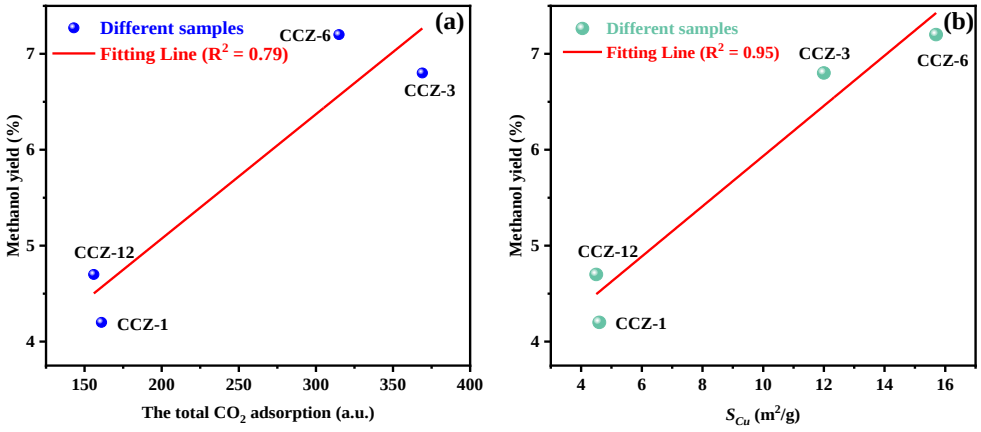

Figure 11. The relationship between the methanol yield and the total CO_2 adsorption (**a**), and the S_{Cu} (**b**).

On the other hand, the S_{Cu} stands as a crucial parameter for copper-based catalysts in methanol synthesis. Researchers have extensively explored the relationship between the catalytic activity of copper-based catalysts and the S_{Cu} [12,42,43]. However, there are conflicting views about their relationship. Natesakhawa et al. [42] reported a linear correlation between the methanol yield and the S_{Cu}. Our previous study [27] also demonstrated a strong link between the S_{Cu} and CO_2 conversion over Cu-$Ce_{1-x}Zr_xO_2$ catalysts in CO_2 hydrogenation to methanol. Conversely, Zhang et al. [43] and Hou et al. [44] found no connection between the methanol yield and the S_{Cu}. In this study, the solvothermal time significantly impacted the S_{Cu} of the Cu-ZnO-ZrO_2 catalysts (Table 1). Figure 11b shows the relationship between the S_{Cu} and the methanol yield. It can be seen that there is a

strong linear correlation between the methanol yield and the S_{Cu} (R^2 = 0.95), indicating that the S_{Cu} of the Cu-ZnO-ZrO_2 catalyst is a determining factor in methanol production. From the above analyses, it is clear that a suitable solvothermal time can promote the uniform growth and high dispersion of Cu particles, and thus increasing the S_{Cu}. This can be confirmed by the results of the XRD, SEM, EDX mapping, N_2O chemisorption, and N_2 adsorption–desorption, as described above.

It is well known that the solvothermal time greatly affects the properties of materials synthesized by the solvothermal method [18,19,45]. During solvothermal synthesis, the reaction time determines the growth rate of the catalyst particles and the interaction between different components. An optimal reaction time can lead to the formation of highly dispersed and well-crystallized catalysts with a large specific surface area, enhancing their catalytic performance. However, an insufficient or excessive reaction time can result in catalysts with poor activity due to incomplete crystallization or excessive particle growth. In our case, as the solvothermal time increased from 1 h to 6 h, the size of the formed CuO particles decreased, as observed from the XRD findings (Figure 1). As a result, the catalysts exhibited a larger S_{BET}, as indicated by the N_2 adsorption–desorption (Figure 3 and Table 1), and the S_{Cu} increased noticeably (Table 1). As the solvothermal time further increased to 12 h, nevertheless, small particles of CuO began to aggregate together and larger particles were formed, as evidenced by the data in Table 1. Consequently, the S_{Cu} was distinctly decreased. Evidently, the CZZ-6 catalyst possesses the largest S_{Cu}, which exhibits a maximal capacity for dissociative adsorption of H_2 (Table 4) and thus the highest CO_2 conversion and methanol yield (Figure 10) among the investigated CZZ-X catalysts. Figure 12 illustrates the effect of the solvothermal time for CO_2 hydrogenation to methanol.

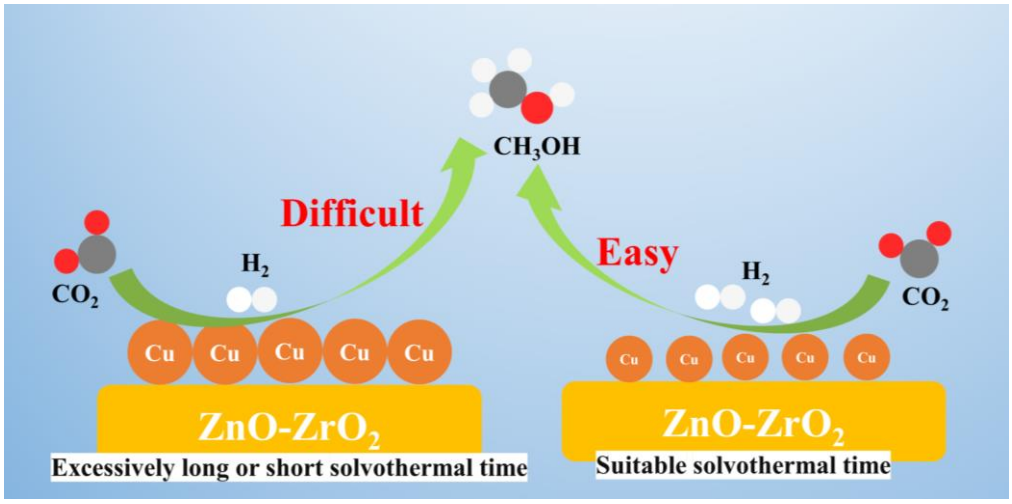

Figure 12. Schematic illustration of the effect of the solvothermal time for CO_2 hydrogenation to methanol.

3. Materials and Methods

3.1. Catalyst Preparation

In this paper, Cu-ZnO-ZrO_2 catalysts with the same molar ratio of Cu/Zn/Zr = 5:2:3 were prepared by the solvothermal method. The choice of this specific molar ratio was made to ensure comparability with our prior studies [16,17] and to build upon the successful results achieved earlier. Firstly, $Cu(NO_3)_2{\cdot}3H_2O$ (AR), $Zn(NO_3)_2{\cdot}6H_2O$ (AR), and $Zr(NO_3)_4{\cdot}5H_2O$ (AR) were dissolved in 50 mL of ethylene glycol to prepare a solution with a total ion concentration of 1 mol/L. After stirring and dissolving, the solution was transferred to a reaction kettle and placed in an oven at 180 °C for a certain period (1 h, 3 h, 6 h, and 12 h). After the reaction, the kettle was cooled to room temperature, and the obtained precipitate was filtered, washed thoroughly with anhydrous ethanol and deionized water, and dried overnight in an oven at 120 °C. The yields of the solid products

obtained at different solvothermal times were not noticeably different. Finally, the dried product was calcined at 450 °C for 3 h in a muffle furnace. Both the heating rate during the solvothermal process and the calcination process were set to 5 °C/min. The obtained catalysts were named as CZZ-X, where X represents the solvothermal synthesis time.

3.2. Characterization

X-ray diffraction analysis (XRD) of the catalysts was conducted using a Bruker D8 ADVANCE diffractometer (Karlsruhe, Germany) with Cu Kα radiation. The scanning range was set from 10° to 80° at a scan rate of 10°/min.

Scanning Electron Microscopy (SEM) and (Energy-dispersive X-ray spectroscopy) (EDX) mapping data of samples were gained on Hitachi SU8010 (Tokyo, Japan).

N_2 adsorption–desorption experiments were performed using an ASAP 2020 HD88 instrument (Norcross, GA, USA). The specific surface area and pore volume of the samples were calculated by the Brunauer–Emmett–Teller (BET) and Barrett–Joyner–Halenda (BJH) models, respectively.

The copper surface area (S_{Cu}) was determined using two-step H_2-TPR. Initially, 0.1 g of catalyst was purged with N_2 at 300 °C for 60 min. The first reduction was then performed in a 10 vol% H_2/N_2 mixture to 300 °C. After the reduction, the sample was cooled to 60 °C, purged with N_2 for 30 min, oxidized in 2 vol% N_2O/He for 1 h to ensure the complete oxidation of surface metallic Cu to Cu_2O, and then purged with N_2 for another 30 min. Finally, the catalyst was again reduced to 500 °C in the 10 vol% H_2/N_2 mixture. The S_{Cu} was calculated using the formula:

$$S_{Cu} = \frac{(2X \times N)}{(1.46 \times 10^{19} \times W)} \quad (1)$$

where X is the amount of H_2 consumed during the second TPR process, N is Avogadro's number (6.02×10^{23} atoms/mol), and W is the weight of the catalyst (g).

X-ray photoelectron spectroscopy (XPS) analysis was conducted using an ESCALAB 250Xi spectrometer from Thermo Scientific (Waltham, MA, USA), with Al Kα as the excitation source, and the binding energy of the measured elements was calibrated to C 1 s (284.6 eV).

The H_2 temperature-programmed reduction (H_2-TPR) was used to evaluate the reducibility of the catalysts. The catalyst (30 mg) was pretreated in N_2 at 300 °C for 1 h to remove the surface-adsorbed water and impurities, then cooled to 50 °C. Subsequently, the sample was exposed to the 10 vol% H_2/N_2 mixture until the chromatographic baseline stabilized, followed by heating to 600 °C while monitoring the consumption of H_2 with a thermal conductivity detector (TCD).

The temperature-programmed desorption of H_2 and CO_2 (H_2/CO_2-TPD) was used to characterize the adsorption property of the catalysts. Prior to CO_2 adsorption, the catalyst was reduced at 300 °C for 1 h in a 10 vol% H_2/N_2 mixture. The sample was then cooled to 50 °C, saturated with 10 vol% CO_2/N_2 for 30 min, purged with He for 30 min to remove physically adsorbed CO_2 molecules, and subjected to CO_2-TPD under He flow from 50 °C to 600 °C, with CO_2 signal detection using a mass spectrometer (Pfeiffer Vacuum Quadstar, 32-bit, Aßlar, Germany). The procedures for the H_2-TPD and CO_2-TPD were similar, with the only difference being the replacement of the adsorbed 10 vol% CO_2/N_2 gas to 10 vol% H_2/N_2, and the signal detection was performed using TCD. It should be noted that the TPD experiments for CO_2 and H_2 were conducted on different charges of the sample to ensure independent and accurate analysis of each gas's adsorption and desorption behavior. Fresh samples were used for each TPD experiment, allowing for precise monitoring of the desorbed species without interference from previous gas exposures.

3.3. Activity Tests

A schematic diagram of the reaction apparatus for CO_2 hydrogenation to methanol is illustrated in Figure S1. Different catalysts for CO_2 hydrogenation were evaluated for their activity and selectivity using a continuous-flow fixed-bed reactor. Here, 0.3 g of catalyst with a particle

size of 40–60 mesh was loaded into a stainless-steel reactor with an inner diameter of 5 mm. The catalyst was reduced in a 10 vol% H_2/N_2 stream at 300 °C for 3 h. Subsequently, the reaction was conducted at 240 °C, a pressure of 3 MPa, and a space velocity of 2400 mL/(g_{cat}·h). After a stable reaction period, the products were analyzed using gas chromatography. Under the experimental conditions, the products of the CO_2 hydrogenation reaction included CO and methanol, along with unreacted CO_2 and N_2. No other by-products were detected. The effluent from the reaction was analyzed online using an Agilent 6820 gas chromatograph. Methanol was detected using a flame ionization detector (FID) with a Porapak Q capillary column, while CO, CO_2, and N_2 were detected using a TCD equipped with a carbon molecular sieve column. The CO_2 conversion, product selectivity, and methanol yield were calculated using the following formulas:

$$\text{CO}_2 \text{ conversion } (\%) = \frac{A_{CO} \cdot f_{CO} + A_{CH_3OH} \cdot f_{CH_3OH}}{A_{CO} \cdot f_{CO} + A_{CH_3OH} \cdot f_{CH_3OH} + A_{CO_2} \cdot f_{CO_2}} \quad (2)$$

$$\text{Methanol selectivity}(\%) = \frac{A_{CH_3OH} \cdot f_{CH_3OH}}{A_{CO} \cdot f_{CO} + A_{CH_3OH} \cdot f_{CH_3OH}} \quad (3)$$

$$\text{CO selectivity}(\%) = \frac{A_{CO} \cdot f_{CO}}{A_{CO} \cdot f_{CO} + A_{CH_3OH} \cdot f_{CH_3OH}} \quad (4)$$

$$\text{Methanol yield}(\%) = \text{CO}_2 \text{ conversion} \times \text{Methanol selectivity} \times 100 \quad (5)$$

In the above formulas, A_i denotes the integrated peak area of each substance in the gas chromatographic analysis at the reactor outlet and f_i denotes the correction factor of each substance with respect to N_2.

4. Conclusions

The Cu-ZnO-ZrO_2 catalysts were prepared by the solvothermal method. The effects of different solvothermal times (1 h, 3 h, 6 h, and 12 h) on the physicochemical properties of the Cu-ZnO-ZrO_2 catalysts were investigated. The results of the catalytic activity test revealed that the CZZ-6 exhibited the highest catalytic activity and methanol yield at a solvothermal time of 6 h. It can be observed that the solvothermal treatment time directly affected the size of the catalyst particles and the surface area, which in turn affected the surface properties and the distribution of active sites. The high activity of the CZZ-6 is ascribed to a suitable solvothermal time that promotes the uniform growth and high dispersion of Cu particles and increases the S_{Cu}. This work provides an in-depth study of the regulation of the solvothermal time on Cu-ZnO-ZrO_2 catalysts prepared by the solvothermal method, which provides valuable guidance for high-performance catalysts.

Supplementary Materials: The following supporting information can be downloaded at https://www.mdpi.com/article/10.3390/catal14060390/s1, Figure S1: Schematic diagram of the reaction apparatus for CO_2 hydrogenation to methanol; Table S1: Peak area parameters of the different Cu-ZnO-ZrO_2 catalysts; Table S2: XPS parameters of the different Cu-ZnO-ZrO_2 catalysts; Table S3: Comparison of the activity of the Cu-Zn-Zr catalysts [7,11,12,15,21,24,46–54].

Author Contributions: Conceptualization, J.H. and Y.L.; methodology, J.H. and Y.L.; validation, G.W. and J.Y.; writing—original draft preparation, J.H. and Y.L.; writing—review and editing, J.H. and D.M.; visualization, J.H.; supervision, G.W. and J.Y.; project administration, D.M.; funding acquisition, D.M. All authors have read and agreed to the published version of the manuscript.

Funding: This research was funded by the Shanghai Municipal Science and Technology Commission of China, grant number 23010504600.

Data Availability Statement: Data are contained within the article or Supplementary Materials.

Conflicts of Interest: The authors declare no conflicts of interest.

References

1. Alvarez, A.; Bansode, A.; Urakawa, A.; Bavykina, A.V.; Wezendonk, T.A.; Makkee, M.; Gascon, J.; Kapteijn, F. Challenges in the greener production of formates/formic acid, methanol, and DME by heterogeneously catalyzed CO_2 hydrogenation processes. *Chem. Rev.* **2017**, *117*, 9804–9838. [CrossRef]
2. Porosoff, M.D.; Yan, B.; Chen, J.G. Catalytic reduction of CO_2 by H_2 for synthesis of CO, methanol and hydrocarbons: Challenges and opportunities. *Energy Environ. Sci.* **2016**, *9*, 62–73. [CrossRef]
3. Yang, Z.; Guo, D.; Dong, S.; Wu, J.; Zhu, M.; Han, Y.-F.; Liu, Z.-W. Catalysis for CO_2 hydrogenation—What we have learned/should Learn from the hydrogenation of syngas to methanol. *Catalysts* **2023**, *13*, 1452. [CrossRef]
4. Dang, S.; Yang, H.; Gao, P.; Wang, H.; Li, X.; Wei, W.; Sun, Y. A review of research progress on heterogeneous catalysts for methanol synthesis from carbon dioxide hydrogenation. *Catal. Today* **2019**, *330*, 61–75. [CrossRef]
5. Zhao, L.; Zhang, L.; Wu, Z.; Huang, C.; Chen, K.; Wang, H.; Yang, F. Size effect of Cu particles on interface formation in Cu/ZnO catalysts for methanol synthesis. *Catalysts* **2023**, *13*, 1190. [CrossRef]
6. Witoon, T.; Chalorngtham, J.; Dumrongbunditkul, P.; Chareonpanich, M.; Limtrakul, J. CO_2 hydrogenation to methanol over Cu/ZrO_2 catalysts: Effects of zirconia phases. *Chem. Eng. J.* **2016**, *293*, 327–336. [CrossRef]
7. Witoon, T.; Kachaban, N.; Donphai, W.; Kidkhunthod, P.; Faungnawakij, K.; Chareonpanich, M.; Limtrakul, J. Tuning of catalytic CO_2 hydrogenation by changing composition of $CuO–ZnO–ZrO_2$ catalysts. *Energy Convers. Manag.* **2016**, *118*, 21–31. [CrossRef]
8. Kordus, D.; Widrinna, S.; Timoshenko, J.; Lopez Luna, M.; Rettenmaier, C.; Chee, S.W.; Ortega, E.; Karslioglu, O.; Kuhl, S.; Roldan Cuenya, B. Enhanced methanol synthesis from CO_2 hydrogenation achieved by tuning the Cu-ZnO interaction in ZnO/Cu_2O nanocube catalysts supported on ZrO_2 and SiO_2. *J. Am. Chem. Soc.* **2024**, *146*, 8677–8687. [CrossRef] [PubMed]
9. Zabilskiy, M.; Sushkevich, V.L.; Palagin, D.; Newton, M.A.; Krumeich, F.; van Bokhoven, J.A. The unique interplay between copper and zinc during catalytic carbon dioxide hydrogenation to methanol. *Nat. Commun.* **2020**, *11*, 2409. [CrossRef]
10. Marcos, F.C.F.; Cavalcanti, F.M.; Petrolini, D.D.; Lin, L.; Betancourt, L.E.; Senanayake, S.D.; Rodriguez, J.A.; Assaf, J.M.; Giudici, R.; Assaf, E.M. Effect of operating parameters on H_2/CO_2 conversion to methanol over Cu-Zn oxide supported on ZrO_2 polymorph catalysts: Characterization and kinetics. *Chem. Eng. J.* **2022**, *427*, 130947. [CrossRef]
11. Bonura, G.; Cordaro, M.; Cannilla, C.; Arena, F.; Frusteri, F. The changing nature of the active site of Cu-Zn-Zr catalysts for the CO_2 hydrogenation reaction to methanol. *Appl. Catal. B Environ.* **2014**, *152–153*, 152–161. [CrossRef]
12. Dong, X.; Li, F.; Zhao, N.; Xiao, F.; Wang, J.; Tan, Y. CO_2 hydrogenation to methanol over $Cu/ZnO/ZrO_2$ catalysts prepared by precipitation-reduction method. *Appl. Catal. B Environ.* **2016**, *191*, 8–17. [CrossRef]
13. Witoon, T.; Numpilai, T.; Phongamwong, T.; Donphai, W.; Boonyuen, C.; Warakulwit, C.; Chareonpanich, M.; Limtrakul, J. Enhanced activity, selectivity and stability of a $CuO-ZnO-ZrO_2$ catalyst by adding graphene oxide for CO_2 hydrogenation to methanol. *Chem. Eng. J.* **2018**, *334*, 1781–1791. [CrossRef]
14. Chang, X.; Zi, X.; Li, J.; Liu, F.; Han, X.; Chen, J.; Hao, Z.; Zhang, H.; Zhang, Z.; Gao, P.; et al. An insight into synergistic metal-oxide interaction in CO_2 hydrogenation to methanol over $Cu/ZnO/ZrO_2$. *Catalysts* **2023**, *13*, 1337. [CrossRef]
15. Chen, D.; Mao, D.; Xiao, J.; Guo, X.; Yu, J. CO_2 hydrogenation to methanol over $CuO–ZnO–TiO_2–ZrO_2$: A comparison of catalysts prepared by sol–gel, solid-state reaction and solution-combustion. *J. Sol-Gel Sci. Technol.* **2018**, *86*, 719–730. [CrossRef]
16. Liang, Y.; Mao, D.; Guo, X.; Yu, J.; Wu, G.; Ma, Z. Solvothermal preparation of $CuO-ZnO-ZrO_2$ catalysts for methanol synthesis via CO_2 hydrogenation. *J. Taiwan Inst. Chem. Eng.* **2021**, *121*, 81–91. [CrossRef]
17. Liang, Y.; Han, J.; Yu, J.; Wu, G.; Mao, D. Methanol synthesis from CO_2 hydrogenation on $CuO–ZnO–ZrO_2$ prepared by solvothermal method: The influence of solvent on catalyst properties and catalytic behavior. *Top. Catal.* **2023**, *66*, 1503–1514. [CrossRef]
18. Yang, Y.; Liang, Y.; Zhang, Z.; Zhang, Y.; Wu, H.; Hu, Z. Morphology well-controlled synthesis of NiO by solvothermal reaction time and their morphology-dependent pseudocapacitive performances. *J. Alloys Compd.* **2016**, *658*, 621–628. [CrossRef]
19. Ni, X.; Zhang, J.; Zhao, L.; Wang, F.; He, H.; Dramou, P. Study of the solvothermal method time variation effects on magnetic iron oxide nanoparticles (Fe_3O_4) features. *J. Phys. Chem. Solids* **2022**, *169*, 110855. [CrossRef]
20. Wang, G.; Mao, D.; Guo, X.; Yu, J. Enhanced performance of the $CuO-ZnO-ZrO_2$ catalyst for CO_2 hydrogenation to methanol by WO_3 modification. *Appl. Surf. Sci.* **2018**, *456*, 403–409. [CrossRef]
21. Guo, X.; Mao, D.; Lu, G.; Wang, S.; Wu, G. Glycine–nitrate combustion synthesis of $CuO–ZnO–ZrO_2$ catalysts for methanol synthesis from CO_2 hydrogenation. *J. Catal.* **2010**, *271*, 178–185. [CrossRef]
22. Samson, K.; Śliwa, M.; Socha, R.P.; Góra-Marek, K.; Mucha, D.; Rutkowska-Zbik, D.; Paul, J.F.; Ruggiero-Mikołajczyk, M.; Grabowski, R.; Słoczyński, J. Influence of ZrO_2 structure and copper electronic state on activity of Cu/ZrO_2 catalysts in methanol synthesis from CO_2. *ACS Catal.* **2014**, *4*, 3730–3741. [CrossRef]
23. Shi, L.; Shen, W.; Yang, G.; Fan, X.; Jin, Y.; Zeng, C.; Matsuda, K.; Tsubaki, N. Formic acid directly assisted solid-state synthesis of metallic catalysts without further reduction: As-prepared Cu/ZnO catalysts for low-temperature methanol synthesis. *J. Catal.* **2013**, *302*, 83–90. [CrossRef]
24. Huang, C.; Mao, D.; Guo, X.; Yu, J. Microwave-assisted hydrothermal synthesis of $CuO–ZnO–ZrO_2$ as catalyst for direct synthesis of nethanol by carbon dioxide hydrogenation. *Energy Technol.* **2017**, *5*, 2100–2107. [CrossRef]
25. Liu, H.; Huang, W.; Yu, Z.; Wang, X.; Jia, Y.; Huang, M.; Yang, H.; Li, R.; Wei, Q.; Zhou, Y. High-performance CuMgAl catalysts derived from hydrotalcite for CO_2 hydrogenation to methanol: Effects of Cu-MgO interaction. *Mol. Catal.* **2024**, *558*, 114002. [CrossRef]

26. Xue, H.; Guo, X.; Mao, D.; Meng, T.; Yu, J.; Ma, Z. Phosphotungstic acid-modified MnO_x for selective catalytic reduction of NO_x with NH_3. *Catalysts* **2022**, *12*, 1248. [CrossRef]
27. Han, J.; Yu, J.; Xue, Z.; Wu, G.; Mao, D. Highly efficient CO_2 hydrogenation to methanol over Cu–$Ce_{1-x}Zr_xO_2$ catalysts prepared by an eco-friendly and facile solid-phase grinding method. *Renew. Energy* **2024**, *222*, 119951. [CrossRef]
28. Wang, H.; Zhang, G.; Fan, G.; Yang, L.; Li, F. Fabrication of Zr–Ce oxide solid solution surrounded Cu-based catalyst assisted by a microliquid film reactor for efficient CO_2 hydrogenation to produce methanol. *Ind. Eng. Chem. Res.* **2021**, *60*, 16188–16200. [CrossRef]
29. Sripada, P.; Kimpton, J.; Barlow, A.; Williams, T.; Kandasamy, S.; Bhattacharya, S. Investigating the dynamic structural changes on Cu/CeO_2 catalysts observed during CO_2 hydrogenation. *J. Catal.* **2020**, *381*, 415–426. [CrossRef]
30. Hu, X.; Mao, D.; Yu, J.; Xue, Z. Low-temperature CO oxidation on CuO-CeO_2-ZrO_2 catalysts prepared by a facile surfactant-assisted grinding method. *Fuel* **2023**, *340*, 127529. [CrossRef]
31. Chen, G.; Yu, J.; Li, G.; Zheng, X.; Mao, H.; Mao, D. Cu^+-ZrO_2 interfacial sites with highly dispersed copper nanoparticles derived from Cu@UiO-67 hybrid for efficient CO_2 hydrogenation to methanol. *Int. J. Hydrogen Energy* **2023**, *48*, 2605–2616. [CrossRef]
32. Cui, X.; Yan, W.; Yang, H.; Shi, Y.; Xue, Y.; Zhang, H.; Niu, Y.; Fan, W.; Deng, T. Preserving the active Cu–ZnO interface for selective hydrogenation of CO_2 to dimethyl ether and methanol. *ACS Sustain. Chem. Eng.* **2021**, *9*, 2661–2672. [CrossRef]
33. Wang, W.; Qu, Z.; Song, L.; Fu, Q. An investigation of Zr/Ce ratio influencing the catalytic performance of CuO/$Ce_{1-x}Zr_xO_2$ catalyst for CO_2 hydrogenation to CH_3OH. *J. Energy Chem.* **2020**, *47*, 18–28. [CrossRef]
34. Wang, W.; Zhang, X.; Guo, M.; Li, J.; Peng, C. An investigation of the CH_3OH and CO selectivity of CO_2 hydrogenation over Cu−Ce−Zr catalysts. *Front. Chem. Sci. Eng.* **2022**, *16*, 950–962. [CrossRef]
35. Wang, W.; Qu, Z.; Song, L.; Fu, Q. CO_2 hydrogenation to methanol over Cu/CeO_2 and Cu/ZrO_2 catalysts: Tuning methanol selectivity via metal-support interaction. *J. Energy Chem.* **2020**, *40*, 22–30. [CrossRef]
36. Wang, Y.; Kattel, S.; Gao, W.; Li, K.; Liu, P.; Chen, J.G.; Wang, H. Exploring the ternary interactions in Cu-ZnO-ZrO_2 catalysts for efficient CO_2 hydrogenation to methanol. *Nat. Commun.* **2019**, *10*, 1166. [CrossRef] [PubMed]
37. Mao, D.; Zhang, H.; Zhang, J.; Wu, D. The influence of the compositions and structures of Cu-ZrO_2 catalysts on the catalytic performance of CO_2 hydrogenation to CH_3OH. *Chem. Eng. J.* **2023**, *471*, 144605. [CrossRef]
38. Song, L.; Wang, H.; Wang, S.; Qu, Z. Dual-site activation of H_2 over $Cu/ZnAl_2O_4$ boosting CO_2 hydrogenation to methanol. *Appl. Catal. B Environ.* **2023**, *322*, 122137. [CrossRef]
39. An, B.; Zhang, J.; Cheng, K.; Ji, P.; Wang, C.; Lin, W. Confinement of ultrasmall Cu/ZnO_x nanoparticles in metal–organic frameworks for selective methanol synthesis from catalytic hydrogenation of CO_2. *J. Am. Chem. Soc.* **2017**, *139*, 3834–3840. [CrossRef]
40. Dasireddy, V.D.B.C.; Likozar, B. The role of copper oxidation state in $Cu/ZnO/Al_2O_3$ catalysts in CO_2 hydrogenation and methanol productivity. *Renew. Energy* **2019**, *140*, 452–460. [CrossRef]
41. Singh, R.; Kundu, K.; Pant, K.K. CO_2 hydrogenation to methanol over Cu-ZnO-CeO_2 catalyst: Reaction structure–activity relationship, optimizing Ce and Zn ratio, and kinetic study. *Chem. Eng. J.* **2024**, *479*, 147783. [CrossRef]
42. Natesakhawat, S.; Lekse, J.W.; Baltrus, J.P.; Ohodnicki, P.R.; Howard, B.H.; Deng, X.; Matranga, C. Active sites and structure–activity relationships of copper-based catalysts for carbon dioxide hydrogenation to methanol. *ACS Catal.* **2012**, *2*, 1667–1676. [CrossRef]
43. Zhang, C.; Wang, L.; Etim, U.J.; Song, Y.; Gazit, O.M.; Zhong, Z. Oxygen vacancies in Cu/TiO_2 boost strong metal-support interaction and CO_2 hydrogenation to methanol. *J. Catal.* **2022**, *413*, 284–296. [CrossRef]
44. Hou, X.-X.; Xu, C.-H.; Liu, Y.-L.; Li, J.-J.; Hu, X.-D.; Liu, J.; Liu, J.-Y.; Xu, Q. Improved methanol synthesis from CO_2 hydrogenation over CuZnAlZr catalysts with precursor pre-activation by formaldehyde. *J. Catal.* **2019**, *379*, 147–153. [CrossRef]
45. Huang, J.F.; Zhu, J.; Cao, L.Y.; Fei, J.; Wu, J.P. Influence of solvothermal time on oxidation resistance of carbon/carbon composites modified by borate sol. *Surf. Eng.* **2012**, *28*, 351–356. [CrossRef]
46. Raudaskoski, R.; Niemelä, M.V.; Keiski, R.L. The effect of ageing time on co-precipitated $Cu/ZnO/ZrO_2$ catalysts used in methanol synthesis from CO_2 and H_2. *Top. Catal.* **2007**, *45*, 57–60. [CrossRef]
47. Zou, T.; Araújo, T.P.; Krumeich, F.; Mondelli, C.; Pérez-Ramírez, J. ZnO-promoted inverse ZrO_2–Cu catalysts for CO_2-based methanol synthesis under mild conditions. *ACS Sustain. Chem. Eng.* **2021**, *10*, 81–90. [CrossRef]
48. Angelo, L.; Girleanu, M.; Ersen, O.; Serra, C.; Parkhomenko, K.; Roger, A.-C. Catalyst synthesis by continuous coprecipitation under micro-fluidic conditions: Application to the preparation of catalysts for methanol synthesis from CO_2/H_2. *Catal. Today* **2016**, *270*, 59–67. [CrossRef]
49. Arena, F.; Barbera, K.; Italiano, G.; Bonura, G.; Spadaro, L.; Frusteri, F. Synthesis, characterization and activity pattern of Cu–ZnO/ZrO_2 catalysts in the hydrogenation of carbon dioxide to methanol. *J. Catal.* **2007**, *249*, 185–194. [CrossRef]
50. Ding, Z.; Xu, Y.; Yang, Q.; Hou, R. Pd-modified CuO–ZnO–ZrO_2 catalysts for CH_3OH synthesis from CO_2 hydrogenation. *Int. J. Hydrogen Energy* **2022**, *47*, 24750–24760. [CrossRef]
51. Ma, Y.; Sun, Q.; Wu, D.; Fan, W.-H.; Zhang, Y.-L.; Deng, J.-F. A practical approach for the preparation of high activity $Cu/ZnO/ZrO_2$ catalyst for methanol synthesis from CO_2 hydrogenation. *Appl. Catal. A Gen.* **1998**, *171*, 45–55. [CrossRef]
52. Li, L.; Mao, D.; Yu, J.; Guo, X. Highly selective hydrogenation of CO_2 to methanol over CuO–ZnO–ZrO_2 catalysts prepared by a surfactant-assisted co-precipitation method. *J. Power Sources* **2015**, *279*, 394–404. [CrossRef]

53. Marcos, F.C.F.; Lin, L.; Betancourt, L.E.; Senanayake, S.D.; Rodriguez, J.A.; Assaf, J.M.; Giudici, R.; Assaf, E.M. Insights into the methanol synthesis mechanism via CO_2 hydrogenation over Cu-ZnO-ZrO_2 catalysts: Effects of surfactant/Cu-Zn-Zr molar ratio. *J. CO2 Util.* **2020**, *41*, 101215. [CrossRef]
54. Li, Z.; Du, T.; Li, Y.; Jia, H.; Wang, Y.; Song, Y.; Fang, X. Water-and reduction-free preparation of oxygen vacancy rich Cu-ZnO-ZrO_2 catalysts for promoted methanol synthesis from CO_2. *Fuel* **2022**, *322*, 124264. [CrossRef]